https://doi.org/10.5194/egusphere-2026-6385
Preprint. Discussion started: 30 October 2026
© Author(s) 2026. CC BY 4.0 License.

Tropopause structure and biases in climate models related to stratospheric water vapour

Felix Ploeger[1,2], Amelie Mayer[1], Helena Eckstein[1], Hongyue Wang[1], Sean Davis[3], and Thomas Birner[4]

[1]Institute of Climate and Energy Systems, Stratosphere (ICE–4), Forschungszentrum Jülich, Jülich, Germany.
[2]Institute for Atmospheric and Environmental Research, University of Wuppertal, Wuppertal, Germany.
[3]NOAA Chemical Sciences Laboratory, Boulder, CO, USA.
[4]Meteorological Institute Munich, Ludwig Maximilians University of Munich, Munich, Germany.

Correspondence: Felix Ploeger (f.ploeger@fz-juelich.de)

Abstract. The thermal tropopause, which marks the transition between the troposphere below and the stratosphere above, is a key indicator of the thermal structure of the upper troposphere and lower stratosphere (UTLS), and changes in tropopause structure are closely linked to changes in atmospheric circulation. Here, we analyze climate model simulations from two model intercomparison projects (CCMI–2022, CMIP6) and from targeted simulation experiments with the ECHAM MESSy Atmospheric Chemistry model (EMAC) and compare to ERA5 reanalysis and satellite observations. Consistent with previous analyses we find that climate models systematically place the extratropical thermal tropopause too high, yielding tropopause pressures lower than observed. These tropopause biases are associated with a cold bias in the lowermost stratosphere, which itself appears to be related to a moist bias in this region. In particular, the sensitivity of extratropical tropopause pressure to changes in water vapour mixing ratios in the lowermost stratosphere (LMS) estimated from multi-model statistics agrees well with the sensitivity predicted from the targeted simulation experiments. Seasonal and inter-annual variability in the pressure level of the extratropical tropopause is found to be slightly underestimated in the model simulations, while trends over past decades show a stronger tropopause rise in models than in the reanalysis. Model projections of future tropopause trends depend strongly on the emission scenario and show substantial spread between the different climate models. We conclude that addressing moist biases in the lowermost stratosphere is essential for reliable simulation of the thermal structure of the UTLS and the tropopause in climate models.

1 Introduction

The tropopause represents the transition level between the troposphere below and the stratosphere above and is surrounded by a transition layer where the characteristics of air mass composition and atmospheric dynamics gradually change from tropospheric to stratospheric. In the tropics, the tropopause is located at relatively high altitudes of about 16 km, corresponding

https://doi.org/10.5194/egusphere-2026-6385
Preprint. Discussion started: 30 October 2026
© Author(s) 2026. CC BY 4.0 License.

to low pressure levels of around 100 hPa. On average, the tropopause slopes downwards towards high latitudes, where it reaches an altitude of about 10 km, corresponding to a pressure level around 250 hPa (e.g. Gettelman et al., 2011).

The tropopause can be defined from a number of different perspectives, including as the interface between atmospheric regions characterized by distinct thermal structures, dynamical behaviour, and chemical composition. First, if viewed as transition level between distinct thermal structures, the tropopause can be described as a level of a specific change in temperature lapse rate or as the level of the temperature minimum. This study uses the standard lapse rate definition according to WMO (1957), which is the most widely used tropopause definition, can be readily applied globally and requires only temperature fields in observational or model data (for further details see Sect. 2.3). This definition exploits the fact that temperatures typically decrease with altitude in the troposphere and increase in the stratosphere, resulting in a reversal of the lapse rate around the tropopause. A recent study has shown that defining the thermal tropopause using the vertical gradient of potential temperature may provide an alternative metric for identifying the sharpest transition in atmospheric composition (Tinney et al., 2022). Second, if viewed as transition level between regimes of different dynamical behaviour, the tropopause is typically defined by a change in potential vorticity (PV). Accordingly, the tropopause can be either diagnosed as a fixed PV contour (often 2 PVU, see Holton et al., 1995) or by a maximum in the isentropic PV-gradient (Kunz et al., 2011; Turhal et al., 2024). Third, from a chemical viewpoint the tropopause can also be defined as a surface of a given value in tracer mixig ratio (e.g. O_3, N_2O, see Bethan et al., 1996; Bauchinger et al., 2025) or its gradient (Schmidt et al., 2010), while microphysical definitions can involve ice water content (Reutter and Spichtinger, 2025).

Tropopause structure and changes therein are of particular relevance for atmospheric large-scale circulation. A recent study by Boljka and Birner (2022) has shown that an increase in tropopause sharpness, indicated by an increased static stability just above the extratropical tropopause in the Tropopause Inversion Layer (TIL, Birner et al., 2002), is linked to an intensified general circulation and equatorward shifted tropospheric jet. Their results indicate that this relation holds across multi-model statistics as well as for inter-annual variability in reanalysis data. Based on a suite of many different climate model simulations and an indealized model experiment, Lorenz and DeWeaver (2007) investigated links between tropopause height and the location of the tropospheric jet in a future climate. They argued that there is a close connection between the poleward shift of the jet streams and a rise in the height of the extratropical tropopause with global warming.

Early studies demonstrated that the height of the tropopause is largely controlled by the transition from a dynamically active troposphere to a stratosphere in radiative equilibrium, with baroclinic eddies exerting a particularly important influence on tropopause structure (Held, 1982). Subsequent studies focused on the roles of more specific processes, including the stirring effects of baroclinic eddies (Haynes et al., 2001), the radiative impacts of individual chemical species (Thuburn and Craig, 2000), and the influence of stratospheric circulation (Birner, 2010; Haqq-Misra et al., 2011). It is the interplay of all these different processes which controls the height of the tropopause, with the relative contributions differing between the tropics and extratropics, as well as between climatological states and long-term trends. Over recent decades, observations have revealed an increase in global tropopause height (e.g. Homeyer and Tinney, 2026), with this trend being closely linked to stratospheric cooling (Seidel and Randel, 2006) and representing a fingerprint of climate change. Under future global warming, climate models likewise project a rising tropopause, primarily driven by an increase in water vapour path, the vertically integrated

https://doi.org/10.5194/egusphere-2026-6385
Preprint. Discussion started: 30 October 2026
© Author(s) 2026. CC BY 4.0 License.

amount of water vapour in the atmospheric column, and a reduction in the tropospheric lapse rate (Hu and Vallis, 2019). Given the various links between tropopause changes and atmospheric circulation discussed above, these tropopause trends represent an important component of the changing climate system.

The temperature minimum in the vicinity of the tropical tropopause plays a key role in regulating stratospheric water vapour mixing ratios (e.g. Brewer, 1949). When moist tropospheric air masses ascend through the tropopause region, cooling induces ice cloud formation that reduces water vapour concentrations to the low saturation mixing ratios associated with the cold temperatures (e.g. Fueglistaler et al., 2005) and the freeze-drying signal propagates into the global stratosphere (**?**). Sedimentation of the resulting ice particles then dehydrates the air, allowing extremely dry air to enter the stratosphere. In the extratropical lowermost stratosphere, a variety of processes influence the water vapour content, including the large-scale stratospheric circulation and isentropic mixing (e.g. Ploeger et al., 2013), local convection (e.g. Homeyer et al., 2023; Ueyama et al., 2023), transport within monsoon circulations and export to high-latitudes (e.g. Nützel et al., 2019; Rolf et al., 2018; Park et al., 2021).

Research over the last one to two decades has shown that models struggle to accurately simulate the water vapour content of the lowermost stratosphere as well as the height and sharpness of the extratropical tropopause. In particular, earlier generations of climate models exhibited a high bias in extratropical tropopause height, corresponding to a low bias in tropopause pressure, as well as a moist bias in water vapour concentrations in the extratropical lowermost stratosphere (Gettelman et al., 2010; Hegglin et al., 2010). More recently, substantial moist biases throughout the lowermost stratosphere have been found to persist even in state-of-the-art climate model simulations (e.g. Charlesworth et al., 2023; Keeble et al., 2021) and weather forecasts (e.g. Bland et al., 2024). These more recent climate models also exhibit a high bias in tropopause altitude (Abalos et al., 2026) alongside the extratropical moist biases, although the former has not yet been investigated in detail. Given that extratropical lowermost stratospheric water vapour is known to influence temperature and tropopause structure (Randel et al., 2007), this raises the question of whether the moist and tropopause biases in the models are related.

Here, we aim for an improved understanding of climate model biases in tropopause height and their potential causes. Therefore, we investigate a suite of state-of-the-art climate model simulations from the CMIP6 and CCMI–2022 inter-comparison projects and a targeted model experiment with the ECHAM MESSy Atmospheric Chemistry (EMAC) model (for details see Sect. 2) in comparison with reanalysis and satellite observations. The specific research questions raised in this paper are: (i) How well do current climate models simulate the climatological stucture and variability of the thermal tropopause?, and (ii) Are biases in tropopause height, as simulated by climate models, related to biases in stratospheric water vapor? Our results are based on a combination of multi-model statistics and mechanistic analysis using the targeted model experiment.

Following the introduction, Sect. 2 describes the datasets and models used as well as the analysis methods. Thereafter, Sect. 3 focuses on biases in the climatologically mean tropopause pressure. Potential relations of these climatological tropopause biases and biases in stratospheric water vapour are investigated in Sect. 4. Finally, Sect. 5 presents trends in tropopause pressure over past decades and into the future. A discussion of the results and final conclusions are given in Sect. 6.

https://doi.org/10.5194/egusphere-2026-6385
Preprint. Discussion started: 30 October 2026
© Author(s) 2026. CC BY 4.0 License.

2 Data and methods

2.1 Climate model simulations

Tropopause characteristics in climate models are investigated based on simulations from two recent multi-model inter-comparison projects, encompassing a diverse range of climate models: the Coupled Model Intercomparison Project, Phase 6 (CMIP6), and the Chemistry–Climate Model Initiative (CCMI–2022). The CMIP6 activity had been conceived to support the Sixth Assessment of the IPCC (AR6). Here, we use the CMIP6 historical simulations for the period 1979–2014. These simulations are fully coupled with sea-surface temperatures evolving as predicted by the respective ocean model and with external forcings following observations as far as possible (e.g. for solar variability, volcanic aerosols, anthropogenic emissions of GHGs and aerosols). Those models without ozone chemistry include prescribed ozone concentrations. Further details on CMIP6 can be found in Eyring et al. (2016), and references therein. For this study we use data from 44 CMIP6 models which provide the necessary variables (CIESM, INM-CM4-8, BCC-ESM1, INM-CM5-0, MIROC6, MCM-UA-1-0, KIOST-ESM, CMCC-CM2-HR4, HadGEM3-GC31-LL, CESM2-WACCM-FV2, ACCESS-ESM1-5, EC-Earth3-CC, CESM2, EC-Earth3-AerChem, TaiESM1, AWI-CM-1-1-MR, MPI-ESM1-2-HR, MIROC-ES2H, EC-Earth3-Veg-LR, FIO-ESM-2-0, GFDL-ESM4, CESM2-FV2, MPI-ESM1-2-LR, FGOALS-f3-L, UKESM1-0-LL, ACCESS-CM2, NESM3, AWI-ESM-1-1-LR, CMCC-CM2-SR5, MRI-ESM2-0, CanESM5-CanOE, CNRM-ESM2-1, CESM2-WACCM, HadGEM3-GC31-MM, CNRM-CM6-1-HR, IPSL-CM6A-LR, CNRM-CM6-1, NorESM2-MM, CMCC-ESM2, MIROC-ES2L, KACE-1-0-G, NorCPM1, FGOALS-g3, SAM0-UNICON). For the assessment of future trends in Sect. 5 we additionally show CMIP6 data from those models which provide the necessary stratospheric water vapour and tropopause variables for SSP2–4.5, SSP3–7.0 and SSP5–8.5 scenarios.

Simulations within the CCMI–2022 project had been designed and carried out for the WMO/UNEP Scientific Assessment of Ozone Depletion Report 2022 (WMO, 2022). For this study we use the refD1 historical hindcast simulations which cover the period 1960–2018. These simulations have prescribed sea-surface temperatures and sea-ice boundary conditions and greenhouse gas forcings following the CMIP6 historical data (extended to 2018 based on the SSP2–4.5 scenario). Ozone-depleting substances are from the WMO baseline scenario and the stratospheric Quasi-Biennial Oscillation (QBO) is nudged. Further details can be found in Plummer et al. (2021). Here, we use data from the following 10 CCMI–2022 models: EMAC-CCMI2, CMAM, UKESM1-StratTrop, CESM2-WACCM, ACCESS-CM2-Chem, NIWA-UKCA2, SOCOL, CCSRNIES-MIROC32, IPSL-CM6A-ATM-LR-REPROBUS, GEOSCCM. Future trends in Sect. 5 are calculated from refD2 simulations.

Further insights into the relation between model biases in tropopause and stratospheric water vapour are gained from a targeted experiment with the ECHAM/MESSy Atmospheric Chemistry (EMAC) model (Jöckel et al., 2016). This model experiment is described by Charlesworth et al. (2023) and includes two simulations which are based on a T42 spectral resolution (approximately 2.8×2.8 degrees horizontal resolution), 90 levels extending from the surface to 0.01 hPa. The simulations are transient and free-running, but with prescribed sea surface temperatures, radiatively active substances like CO_2 , O_3, N_2O, CFC–11, CFC–12, tropospheric and stratospheric aerosol. Further details on the simulations can be found in Charlesworth et al. (2023).

https://doi.org/10.5194/egusphere-2026-6385
Preprint. Discussion started: 30 October 2026
© Author(s) 2026. CC BY 4.0 License.

In the EMAC control simulation trace gas transport is calculated based on the standard EMAC Flux-Form Semi-Lagrangian transport scheme (denoted "EMAC" in the following), while in the Lagrangian sensitivity simulation ("EMAC–CLaMS" in the following) a fully Lagrangian transport scheme is used to calculate stratospheric water vapour (for further details see Charlesworth et al., 2023). Importantly, Lagrangian transport is only enabled for water vapour above about 270 hPa. Hence, the control and Lagrangian simulations only differ in stratospheric water vapour concentrations above that level and all emerging differences between the simulations, like changes in radiative properties, temperatures, dynamics and circulation, can unambiguously been attributed to these differences. In this way, differencing the EMAC control and Lagrangian simulations enables investigation of the impacts of stratospheric water vapour changes on the formation of the thermal tropopause.

2.2 Observations and reanalysis

The climate model simulations are compared to reanalysis data and satellite observations to investigate model biases. For reanalysis data we use ERA5 from the European Centre for Medium-Range Weather Forecasts (ECMWF) over the period 1979–2023 (Hersbach et al., 2020). The data assimilation system for ERA5 involves the ECMWF Integrated Forecast System, cycle CY41R2, and a 4D-Var assimilation scheme. The original ERA5 data is available hourly and with a spectral T639 resolution, corresponding to a horizontal resolution of about 30 km. For the climatological analyses here, we use ERA5 data truncated to $1\times1^\circ$ latitude-longitude and 6-hourly resolution, but including all original 137 vertical model levels (from the surface to about 0.01 hPa).

Observations of stratospheric water vapour considered in this paper are taken from the Stratospheric Water and OzOne Satellite Homogenized (SWOOSH) database version v02.74. SWOOSH is a merged satellite observation data set, including measurements from several instruments (SAGE-II/III, UARS HALOE, UARS MLS, Aura MLS), and covering the period from about 1984 to present. Here, we use monthly mean zonal mean data gridded on a 5° latitude grid for the period 2000–2014, with this period chosen in order to have rather high observational sampling density and to avoid complicating effects of satellite data changes and volcanic eruptions in the 1990s. Note that for all comparisons between model and observational data we restrict the model data to the observational period. For further details on SWOOSH, including details on the specific instruments and the data homogenization method, see Davis et al. (2016).

2.3 Tropopause calculation

The thermal tropopause is calculated based on the definition by the World Meteorological Organization (WMO, 1957) as "the lowest level at which the lapse rate decreases to $2^\circ C/km$ or less, provided also the average lapse rate between this level and all higher levels within 2 km does not exceed $2^\circ C/km$". For this calculation, we used the respective software from the Chemical Lagrangian model of the Stratosphere, CLaMS (Pommrich et al., 2014).

As the necessary data for several climate model simulations is only available as monthly mean fields on a regular latitude-longitude grid (e.g. for CMIP6), we performed the tropopause calculation on the monthly mean fields. For ERA5 reanalysis and EMAC model data, in which the instantaneous 6-hourly fields are available, we compared the tropopause calculation on monthly mean data to the instantaneous calculation (see Appendix A, Fig. A1). The comparison shows that the differ-

https://doi.org/10.5194/egusphere-2026-6385
Preprint. Discussion started: 30 October 2026
© Author(s) 2026. CC BY 4.0 License.

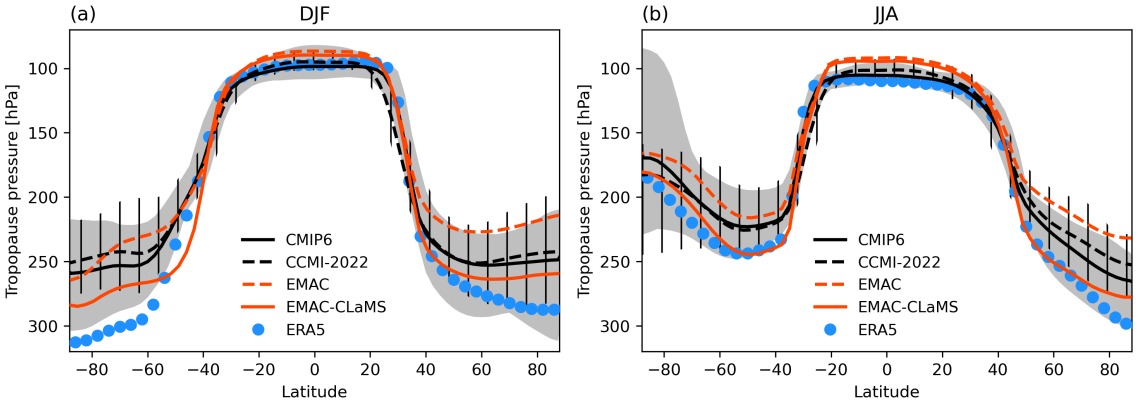

Figure 1. Climatological thermal tropopause pressure during (a) boreal winter (December–February, DJF) and (b) boreal summer (June–August). Data is shown for ERA5 reanalysis (blue dots), from CMIP6 climate models (black solid line the multi-model-mean, grey shading the min-max range), CCMI–2022 models (black dashed, error bars the min-max range), targeted EMAC (red dashed) and EMAC–CLaMS (red solid) simulations.

ences arising from using monthly mean versus instantaneous fields are much smaller than the differences between the various datasets. Furthermore, calculating tropopause characteristics from monthly-mean fields can be advantageous for characterizing the atmospheric background state (cf. Boljka and Birner, 2022), which is the primary focus of this study.

For the climatological analysis, we calculated climatologies over 2000–2014 for ERA5, CMIP6, and CCMI–2022, and over 2000–2009 for EMAC and EMAC–CLaMS, as these simulations were not extended beyond 2009. To examine inter-annual to multi-year variability, we considered the period 1979–2014 for ERA5, CMIP6, and CCMI–2022, and 1990–2009 for EMAC and EMAC–CLaMS.

3 Climatological tropopause structure

Figure 1 shows the latitudinal variability of the climatological zonal mean tropopause pressure from the different climate models compared to ERA5 reanalysis. All datasets exhibit the characteristic pattern of latitudinal tropopause variability, with a higher tropopause in the tropics (corresponding to lower pressure levels) and a lower tropopause at middle and high latitudes (corresponding to higher pressure levels). Comparison of climate model tropopause pressure to reanalysis values shows largest differences in the extratropics, where climate models generally simulate a too high extratropical tropopause. The corresponding low bias in tropopause pressure is a robust feature across the different CMIP6 and CCMI–2022 climate models (Fig. 1).

The tropopause pressure bias is illustrated more clearly in Fig. 2a and b by subtracting ERA5 from the climate model values. Almost all CMIP6 and CCMI–2022 models simulate an extratropical tropopause substantially above the reanalysis tropopause. The tropopause bias is largest in the summer hemisphere, i.e. in the Southern hemisphere during DJF and in the

https://doi.org/10.5194/egusphere-2026-6385
Preprint. Discussion started: 30 October 2026
© Author(s) 2026. CC BY 4.0 License.

Northern hemisphere during JJA. During summer, ERA5 tropopause pressures even fall outside the range represented by the climate models in certain latitude bands. Furthermore, the larger biases are found for CCMI–2022 compared to CMIP6.

The targeted EMAC control simulation shows extratropical tropopause high-biases at the upper end of the distribution of the other climate models (Fig. 2a, b, red dashed). In contrast, the Lagrangian EMAC–CLaMS sensitivity simulation exhibits significantly higher extratropical tropopause pressure levels and a tropopause in much closer agreement with the reanalysis (Figs. 2a, b, red solid).

As shown recently by Charlesworth et al. (2023) and Ploeger et al. (2024), CMIP6 and CCMI–2022 climate models generally simulate significant moist biases in the lowermost stratosphere. These moist biases are illustrated in Fig. 2c and d by subtracting SWOOSH satellite observations from the climate model water vapour mixing ratios averaged over the lowermost stratosphere (150-200 hPa). Clearly, almost all climate models considered simulate a lowermost stratosphere which is too moist, some exceeding SWOOSH observations by up to 500%. The multi-model mean shows a moist bias of a factor two to three compared to the observational reference. The largest moist biases occur in the summer hemisphere and coincide with the maximum tropopause high-biases during the same season (cf. Fig. 2a, b).

The moist bias in the EMAC simulation is at the upper end of the CMIP6 and CCMI–2022 range and even exceeds this range at high latitudes (Fig. 2c, d, red dashed). This moist bias is significantly reduced with the Lagrangian transport scheme of EMAC–CLaMS (see Fig. 2 c, d, red solid, and also Charlesworth et al., 2023; Ploeger et al., 2024). As the only difference between the EMAC control and EMAC–CLaMS Lagrangian simulations is the representation of stratospheric water vapor (see Sect. 2.1), this constitutes the controlling factor for the tropopause height differences between the two simulations. Hence, the rise of the extratropical tropopause in the EMAC control compared to the Lagrangian EMAC–CLaMS simulation can be unambigously attributed to the model moist bias in the extratropical lowermost stratosphere. The relation between the climate model tropopause and moist biases will be further investigated in Sect. 4.

Climate model differences relative to the reanalysis also exist for the potential temperature of the extratropical tropopause, albeit smaller than for tropopause pressure, because a cold bias in tropopause temperature partly compensates for the low bias in tropopause pressure (see Appendix B). Hence, the climate model biases are not merely an artifact of the chosen reference variable but reflect a more fundamental limitation in the models' representation of the extratropical tropopause.

The cold bias in climate model simulations is not confined to the tropopause level but extends throughout the extratropical lowermost stratosphere up to approximately 100 hPa, as shown by presenting mid-latitude temperature profiles in Fig. 3. Note that, for seasonal and monthly means, the latitudinal average here is calculated over 50–70°N/S, rather than 50–90°N/S as used elsewhere, to reduce potential artifacts in tropopause altitude associated with the polar regions of the Southern hemisphere. The largest temperature biases compared to ERA5 reanalysis occur around the 200 hPa pressure level, coinciding with levels of maximum moist biases (cf. Charlesworth et al., 2023). For individual models, temperature biases at these levels may exceed 10K (cf. the lower bound of the CMIP6 range relative to ERA5 in the SH during DJF). In the model simulations, the temperature minimum appears more pronounced than in ERA5, indicating an overly sharp extratropical tropopause, consistent with the findings of Boljka and Birner (2022). This bias in tropopause sharpness in the models is evident in the multi-model mean and is likely even more pronounced for individual models.

https://doi.org/10.5194/egusphere-2026-6385
Preprint. Discussion started: 30 October 2026
© Author(s) 2026. CC BY 4.0 License.

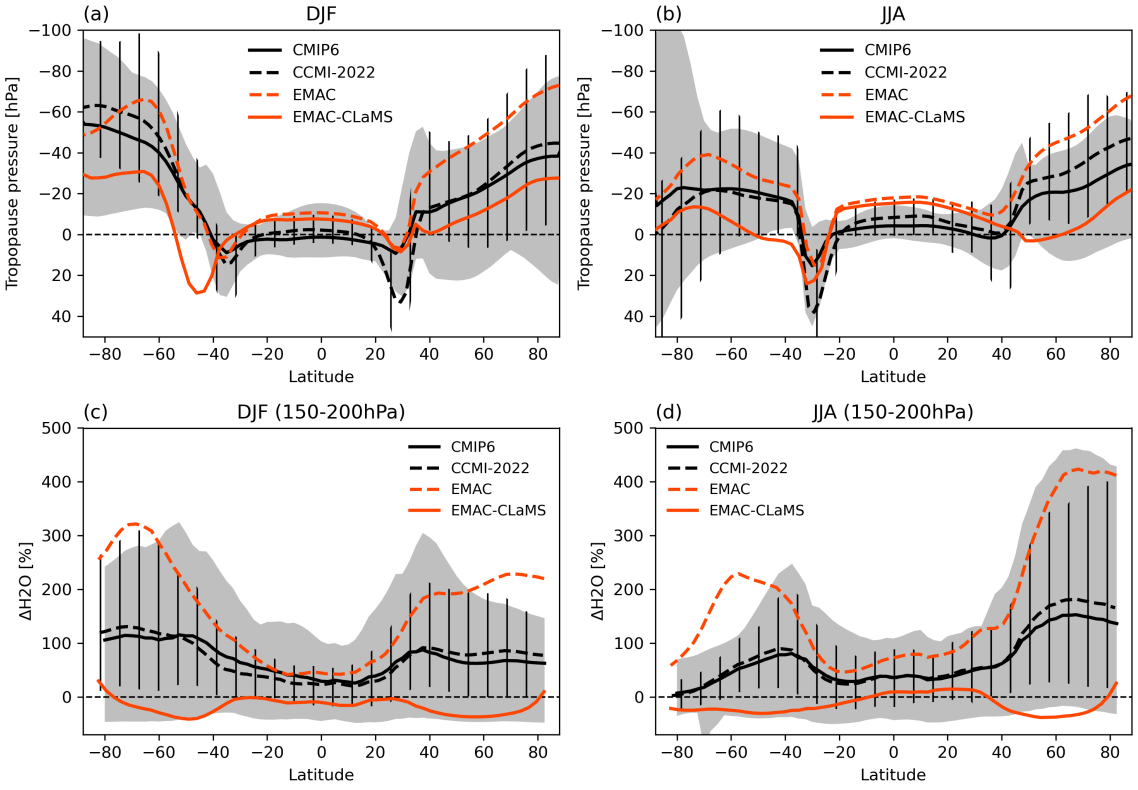

Figure 2. Model bias in climatological thermal tropopause pressure during (a) boreal winter (December–February, DJF) and (b) boreal summer (June–August). The bias is calculated as difference to ERA5 reanalysis and data is shown from CMIP6 climate models (black solid line the multi-model-mean, grey shading the min-max range), CCMI–2022 models (black dashed, error bars the min-max range), targeted EMAC (red dashed) and EMAC–CLaMS (red solid) simulations. (c, d) Water vapour bias in the lowermost stratosphere (150-200 hPa) of the different climate models with respect to SWOOSH merged satellite observations.

While the cold bias in EMAC control is particularly large relative to the other models, the Lagrangian EMAC-CLaMS simulation results in a significant reduction of this bias (Fig. 3). This reduction of the cold bias by use of Lagrangian transport was shown to be related to the reduced moist bias and reduced water vapour longwave cooling (Charlesworth et al., 2023; Ploeger et al., 2024). Still, the temperature minimum appears too sharp and too low also in EMAC–CLaMS, which could be related to the specific simulation set-up in the targeted model experiment. In particular, the choice of the water vapour nudging level of around 270 hPa, below which the control and Lagrangian sensitivity simulations have the same water vapor field (see methods), contributes to a moist bias in the extratropical upper troposphere in the Lagrangian EMAC–CLaMS simulation. Because of this, EMAC–CLaMS long-wave cooling at these lowest levels around the extratropical tropopause is likely too strong. However, as the nudging level is generally below the extratropical tropopause (compare black dashed horizontal line and tropopauses in Fig. 3), water vapour mixing ratios evolve freely throughout the lowermost stratosphere in the simulation.

https://doi.org/10.5194/egusphere-2026-6385
Preprint. Discussion started: 30 October 2026
© Author(s) 2026. CC BY 4.0 License.

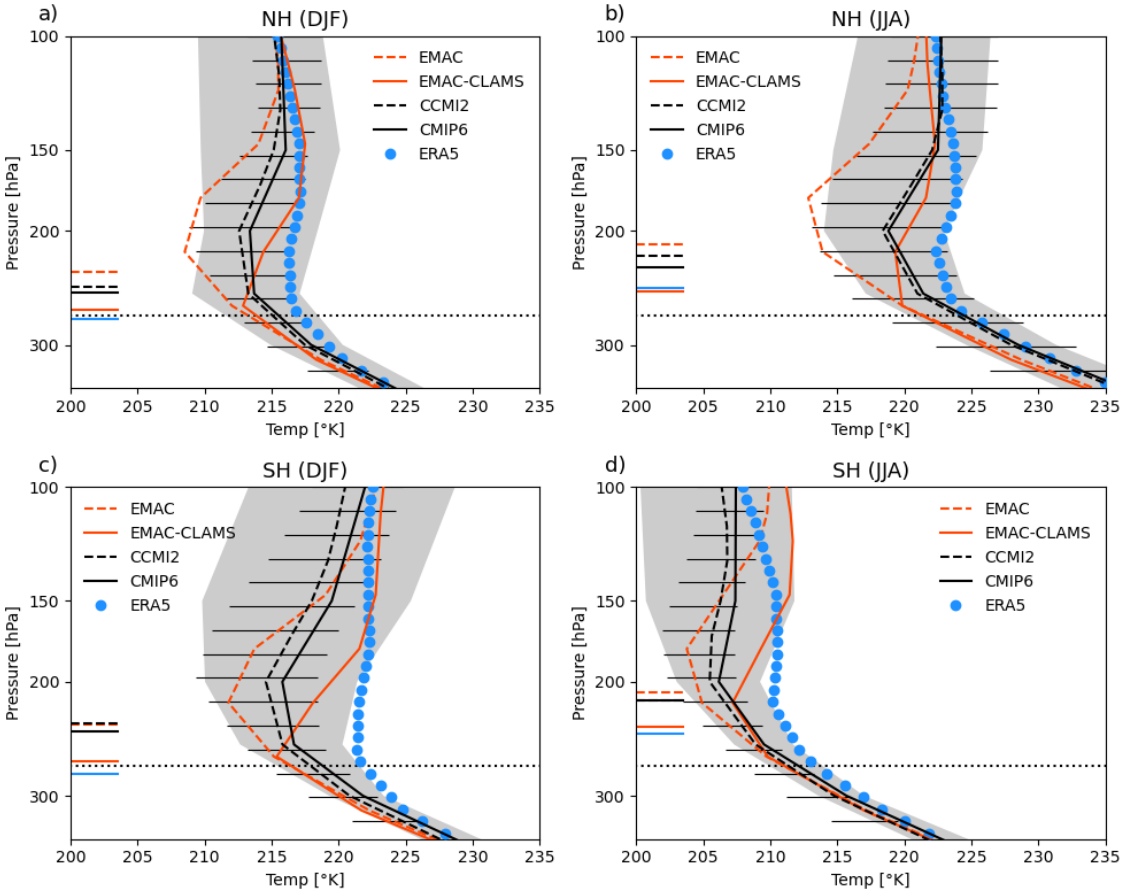

Figure 3. Climatological temperature profiles for boreal winter (December - February, DJF, a and c) and boreal summer (June - August, JJA, b and d) averaged over 50 to 70°N (upper panel) and 50 to 70°S (lower panel). Data shown is from EMAC (red dashed) and EMAC-CLaMS (red solid) simulations, ERA5 reanalysis (blue dots), CCMI-2022 models (multi-model mean as black dashed line, min-max model range as error bars), and CMIP6 models (multi-model mean as black solid line, min-max model range grey shaded). The average tropopause height, according to the WMO definition, is displayed by the horizontal bars on the left side of each panel. The dotted line at 270 hPa indicates the level up to which the EMAC-ClaMS simulation is nudged by the EMAC simulation (see text).

The distribution of the extratropical tropopause pressure for both hemispheres (averaged over 50°-70°N/S) for all climate models considered and ERA5 reanalysis is shown in Fig. 4a. The figure illustrates the robustness of the tropopause pressure low bias. All models except three in the NH simulate tropopause pressures lower than those in the reanalysis, with a multi-model-mean bias around 30 hPa in both hemispheres. The box-whisker plot further indicates that the ERA5 value lies close to the 2σ level of the climate model distribution, and even exceeds it in the SH. The comparison between the two targeted EMAC simulations also shows that the LMS moist bias can cause changes of tropopause pressure in the range of the inter-model

https://doi.org/10.5194/egusphere-2026-6385
Preprint. Discussion started: 30 October 2026
© Author(s) 2026. CC BY 4.0 License.

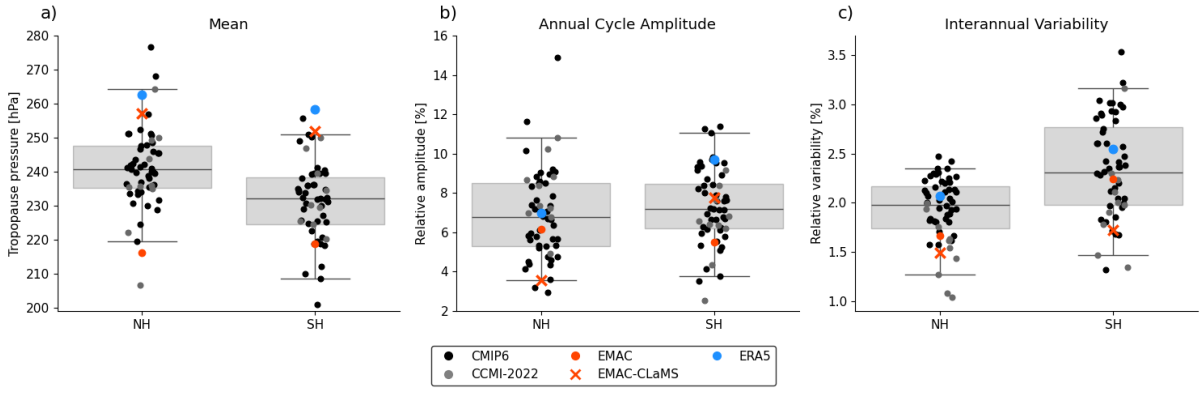

Figure 4. Tropopause pressure (a) climatological mean, (b) seasonal cycle amplitude, and (c) inter-annual variability, for CMIP6 (black), CCMI–2022 (grey) and EMAC (red) climate models, as well as for ERA5 reanalysis (blue). Shown quantities are averages over 50°-70°N/S and have been calculated over the period 1979–2014 (for EMAC simulations over 1990–2009, see methods). Grey shading shows the 25-75% percentile range, whiskers the approximate $\pm 2\sigma$-range of the CMIP6 and CCMI–2022 models. Variability estimates are shown in percent relative to the climatological mean tropopause pressure.

spread. Hence, correcting this bias has the potential to bring the simulated extratropical tropopause into much better agreement with the reanalysis, even for those models with particularly large biases (as e.g. for EMAC).

The distribution of annual cycle amplitudes in Fig. 4b indicates a substantial spread of the climate model values around the reanalysis. In the SH, there is also a slight underestimation of the tropopause pressure annual cycle by the models. The EMAC experiment shows an influence of lowermost stratospheric water vapour also on the tropopause pressure seasonality, but weaker than for the climatological mean state and of different sign in both hemispheres.

Inter-annual variability of extratropical tropopause pressure is calculated over the period 1979–2014 (1990–2009 for EMAC and EMAC–CLaMS) as the standard deviation of the deseasonalized time series, after subtracting the mean seasonal cycle. The distribution in Fig. 4c shows that climate models slightly underestimate inter-annual variability in tropopause pressure, but with a large spread between different models. Furthermore, inter-annual variability appears generally weaker for CCMI–2022 compared to CMIP6 (cf. black and grey points in Fig. 4c), although CCMI–2022 models are newer than CMIP6. This difference could be related to the fact that CCMI–2022 models employ prescribed sea-surface temperatures while CMIP6 models are coupled to an ocean model. Differences in inter-annual variability between the two targeted EMAC simulations are small in the NH and moderate in the SH (red symbols), suggesting that the moist bias in the lowermost stratosphere has a limited impact on tropopause variability. Overall, the distributions in Fig. 4 show that largest biases in extratropical tropopause pressure concern the climatological mean state (tropopause high-bias), while biases in seasonality and inter-annual variability are considerably smaller, showing a slight underestimation of tropopause variability by climate models in certain hemispheres and seasons.

https://doi.org/10.5194/egusphere-2026-6385
Preprint. Discussion started: 30 October 2026
© Author(s) 2026. CC BY 4.0 License.

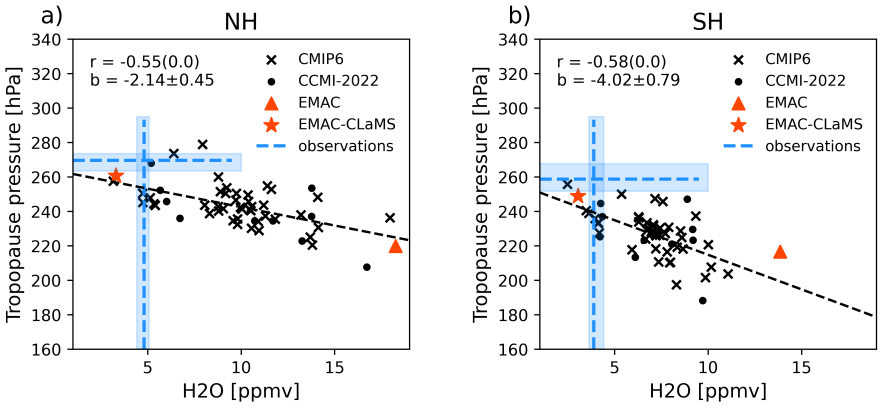

Figure 5. Inter-model correlation of tropopause pressure versus lowermost stratospheric water vapour for (a) NH and (b) SH. The water vapour mixing ratios are averaged over the 150–200 hPa pressure layer and 50°–90° N/S latitude range, and are climatological averages over the entire study period (see Sect. 2). Black symbols are from CMIP6 (historical) and CCMI–2022 (refD1) climate model simulations, blue symbols are from targeted EMAC simulations. Values in the legend are the correlation coefficient (r, with p-value in brackets rounded to two digits) and the regression slope (b, in hPa/ppmv, plus/minus $1-\sigma$ standard error). The blue dashed lines indicate the observational constraints from ERA5 reanalysis for tropopause pressure and from SWOOSH merged satellite dataset for water vapour. Light-blue shading denotes the corresponding uncertainty, defined as the minimum–maximum range of year-to-year variability.

4 Relation between tropopause and stratospheric water vapour

In the following, we analyse statistical relationships across CMIP6 and CCMI–2022 models, in combination with the targeted EMAC model experiment, to further investigate the relation between extratropical tropopause altitude (or similarly pressure) and lowermost stratospheric water vapour. Figure 5 shows that the pressure level of the extratropical tropopause correlates with the water vapour mixing ratio in the lowermost stratosphere (here, averaged over 150-200 hPa) across models, such that models with higher water vapour simulate a lower tropopause pressure (higher tropopause). This correlation is statistically significant with correlation coefficients of -0.55 in the NH and -0.58 in the SH, and a confidence level of at least 95% (p-values below 0.05). The observational constraints (blue dashed lines), being 260-270 hPa for tropopause pressure (from ERA5) and 4-5 ppmv for water vapour (from SWOOSH), lie at the very edge of the model distribution.

A physical mechanism explaining the anti-correlation between tropopause pressure and lowermost stratospheric water vapour is the change in long-wave cooling associated with changes in stratospheric water vapour. Due to induced long-wave cooling, higher water vapour mixing ratios in the lowermost stratosphere are related to lower temperatures in this region, as indicated by a significant anti-correlation between temperature and water vapour in the lowermost stratosphere (see Fig. 6a, d and cf. Charlesworth et al., 2023). Hence, higher water vapour mixing ratios in the lowermost stratosphere cause a sharpened and deepened temperature minimum around the extratropical tropopause (cf. Fig. 3). Lower temperatures in the lowermost stratosphere are, in turn, related to a higher tropopause (lower pressure), as indicated in Fig. 6b, e. Consequently, enhanced

https://doi.org/10.5194/egusphere-2026-6385
Preprint. Discussion started: 30 October 2026
© Author(s) 2026. CC BY 4.0 License.

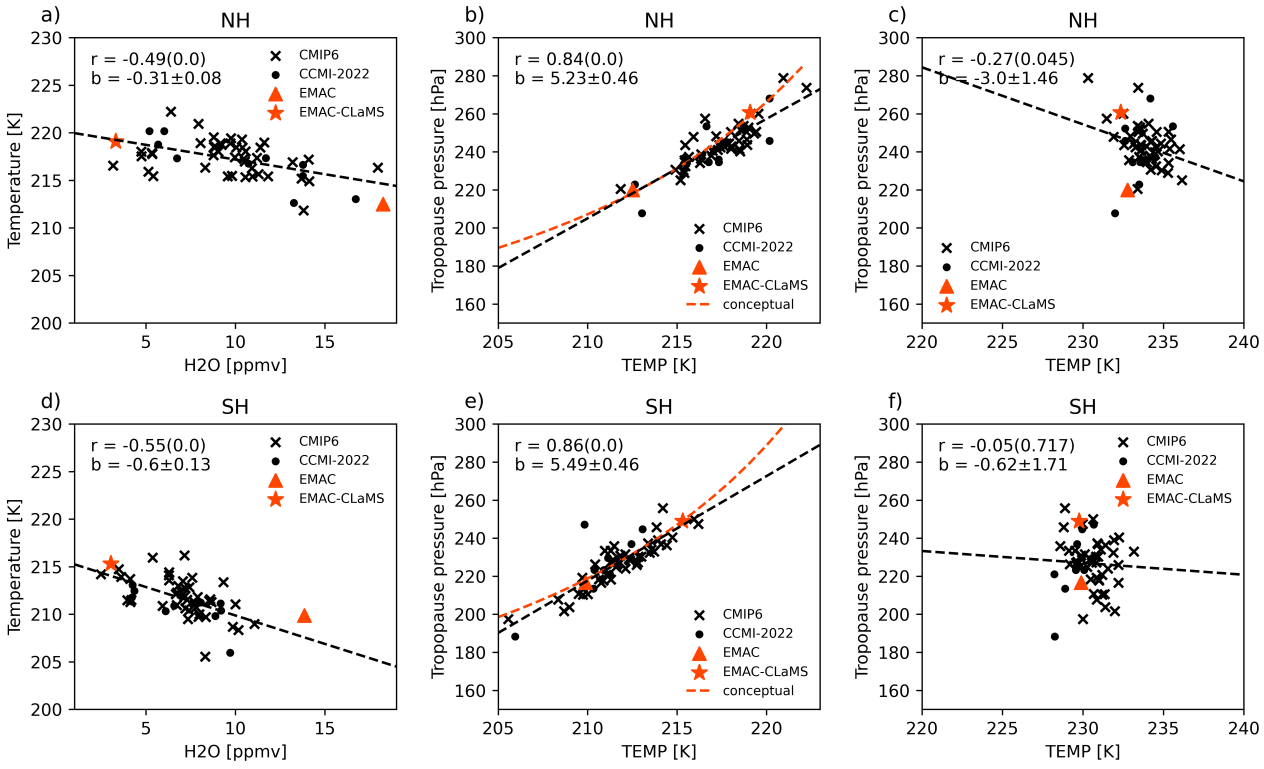

Figure 6. Inter-model correlation of (a, d) lowermost stratospheric temperature and water vapour, (b, e) tropopause pressure versus lowermost stratospheric temperature, and (c, f) tropopause pressure versus upper tropospheric temperature. Upper row shows NH, lower row SH. Lowermost stratosphere values are averaged over the 150–200 hPa pressure layer and 50°–90°N/S latitude range, while upper tropospheric values are averaged over 400 hPa and 50°–90°N/S. Black symbols are from CMIP6 (historical) and CCMI–2022 (refD1) climate model simulations, red symbols are from targeted EMAC simulations. Values in the legend are the correlation coefficient (r, with p-value in brackets rounded to two digits) and the regression slope (b, in hPa/ppmv, plus/minus $1-\sigma$ standard error). The red dashed line (b, e) shows the relation from the conceptual model (see text for details).

water vapour mixing ratios in the lowermost stratosphere are negatively correlated with tropopause pressure, as shown in Fig. 5. The EMAC model experiment clearly shows that this mechanism has the potential to explain the entire inter-model spread of tropopause pressure (compare red symbols in Fig. 5), while the CMIP6 and CCMI–2022 multi-model statistics suggest that the mechanism is also relevant for explaining the differences between the other models.

There is a clear difference between the correlation of tropopause pressure with lowermost stratospheric temperatures and the correlation with upper tropospheric temperatures across models. While tropopause pressure correlates significantly with temperatures in the lowermost stratosphere (correlation coefficient around 0.85, see Fig. 6b, e) there is no significant correlation with temperatures in the upper troposphere (Fig. 6c, f). This finding is consistent with the results of Seidel and Randel

https://doi.org/10.5194/egusphere-2026-6385
Preprint. Discussion started: 30 October 2026
© Author(s) 2026. CC BY 4.0 License.

(2006) who showed that anomalies in tropopause height correlates more closely with stratospheric compared to tropospheric temperatures.

It is clear that tropopause pressure is influenced by different processes amongst which the lowermost stratospheric water vapour mixing ratio χ_{LMS} is only one factor. Denoting these other processes X_i (including tropospheric dynamics, convection, stratospheric ozone and other radiatively active species), the tropopause pressure field is a function of all these variables $p_{\text{trop}}(\chi_{\text{LMS}}, X_i)$. Formally, the "sensitivity" of tropopause pressure with respect to changes in lowermost stratospheric water vapour mixing ratios can be defined as

$$\alpha_{H_2O} = \frac{\partial p_{\text{trop}}}{\partial \chi_{\text{LMS}}} \,. \tag{1}$$

It is this sensitivity of tropopause pressure to stratospheric water vapour changes that is estimated from the differences between the two simulations of the targeted EMAC model experiment as well as from the slope of the multi-model regression. There is good agreement between these two estimates of sensitivity from the multi-model regression and from the EMAC experiment for all relations shown in Fig. 5 and Fig. 6 (compare black dashed lines and difference between red symbols). We see this agreement as a strong hint that the causal effect of a moister lowermost stratosphere raising the extratropical tropopause, which is operating in the EMAC experiment, also holds across the different CMIP6 and CCMI–2022 models. Quantitatively, the sensitivity of tropopause pressure to stratospheric water vapour changes is -2.14 hPa/ppmv in the NH and -4.02 hPa/ppmv in the SH (Fig. 5).

The relation between tropopause pressure and lowermost stratospheric temperature across models as shown in Fig. 6b, e can be understood within an idealized conceptual framework. Motivated by Bland et al. (2024), we assume that the tropospheric and lowermost stratospheric parts of the temperature profile are both characterised by constant lapse rates, and that a cooling perturbation affects temperatures only in the lowermost stratosphere while leaving the profile in the troposphere and in the stratospheric overworld unchanged. In the EMAC experiment, this cooling perturbation is caused by a change in lowermost stratospheric water vapour, while for the CMIP6 and CCMI–2022 model differences such an unambigous attribution is not possible. Consistent with the difference between the two simulations in the EMAC experiment, we assume that the temperature perturbation extends from the tropopause to about 17.5 km with the largest temperature change around 12 km. These assumptions lead to an exponential relation between the tropopause pressure and the temperature in the lowermost stratosphere, as shown in Appendix C and Eq. C2.

Figure 6 shows this conceptual relation between extratropical tropopause pressure and lowermost stratospheric temperature (red dashed line) in comparison to the relation from multi-model statistics. The values from the EMAC experiment (red symbols) lie almost exactly on the conceptual curve, as expected since the parameters of the conceptual model were fitted to the EMAC data. Furthermore, the conceptual model indicates that this relationship holds across the entire temperature range considered. Also, the conceptual relation agrees well with the multi-model statistics, such that the climate models (black symbols) are distributed closely around the conceptual curve. This agreement suggests that the relation of tropopause pressure with LMS temperature across the complex climate models can be understood to first order within a conceptual framework in which the temperature perturbation extends only from the extratropical tropopause to an altitude of approximately 17.5 km, and the lapse

https://doi.org/10.5194/egusphere-2026-6385
Preprint. Discussion started: 30 October 2026
© Author(s) 2026. CC BY 4.0 License.

rate is assumed to be piecewise constant in the troposphere and lowermost stratosphere. The fact that this conceptual framework closely reproduces the multi-model relationship supports the interpretation that LMS cooling, likely driven by water vapour in this region, is a primary factor governing the inter-model spread in tropopause pressure, also in the climate models.

The seasonality of the inter-model relation between extratropical tropopause pressure and lowermost stratospheric water vapour calculated from the multi-model regression for each month is presented in Fig. 7. The correlation turns out to be significant in both hemispheres and throughout all months (except in the SH during winter) and the regression slope exhibits a distinct annual cycle. In particular, the sensitivity of tropopause pressure to stratospheric water vapour changes is largest (most strongly negative) during winter and weakest during summer, with a clearer seasonality in the NH than SH. The insignificant correlation in the SH during winter is likely caused by the interplay of complex dynamical mechanisms affecting the tropopause pressure during that season (e.g. polar vortex variability, stratospheric ozone).

The sensitivity α of tropopause pressure to stratospheric water vapour changes calculated from differencing the EMAC and EMAC–CLaMS targeted simulations is also shown in Fig. 7 (red crosses), for comparison with the multi-model statistics. There is agreement between the seasonality in the sensitivity estimated from the multi-model regression to the estimate from the EMAC experiment, although the seasonal cycle amplitude calculated from the EMAC experiment is somewhat weaker.

The disagreement between the two estimates in the SH during winter and spring (July–October) should not be over-interpreted as the multi-model correlation is not significant during these months and there is large inter-annual variability in both estimates (error bars in Fig. 7). Overall, we consider the agreement between the seasonality of the tropopause sensitivity from both estimates as additional evidence that tropopause differences in the CMIP6 and CCMI climate models are likewise related to differences in lowermost stratospheric water vapour.

5 Tropopause trends

Long-term trends in atmospheric temperature structure and dynamics may also be reflected in trends in tropopause height. Over the past decades, here from 1979 to 2014, climate models simulate a rising tropopause (decreasing tropopause pressure), as shown in Fig. 8a. The tropopause rises more strongly at polar latitudes compared to mid-latitudes and subtropics, with the largest trends observed in the Southern hemisphere. The multi-model mean trends and the inter-model spread are similar for CMIP6 and CCMI–2022 models. Averaged over the extratropics (50°–90°N/S), the multi-model mean tropopause pressure trends from CMIP6 and CCMI-2022 reach about 0.5 %/dec in the NH (corresponding to about 1.5 hPa/dec) and about 1 %/dec in the SH (about 2 hPa/dec), accompanied by a notable inter-model spread (Fig. 8b).

Over the past, climate models simulate larger tropopause trends than represented in ERA5 reanalysis (Fig. 8a, b). In NH polar latitudes the reanalysis trend is almost vanishing and it is even negative in the SH around 60°S, similar to recent findings from Weyland et al. (2025) for a slightly different period. Enhanced trends in the subtropics indicate a substantial tropopause rise in ERA5, strongest in the SH and much weaker in the climate models, and are likely an imprint of tropical widening and a related poleward shift of the tropopause break (e.g. Staten et al., 2018; Turhal et al., 2024). There are several potential reasons for the disagreements in past tropopause trends between climate models and the reanalysis. On the one hand, strong natural variability

https://doi.org/10.5194/egusphere-2026-6385
Preprint. Discussion started: 30 October 2026
© Author(s) 2026. CC BY 4.0 License.

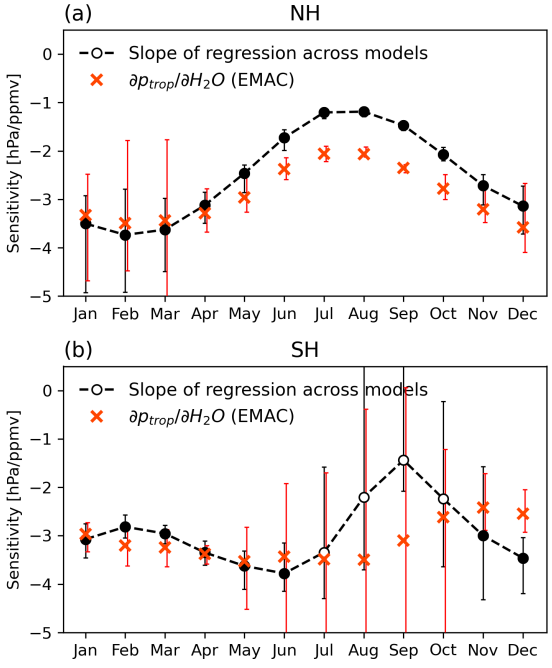

Figure 7. Seasonality of the sensitivity of tropopause pressure with respect to lowermost stratospheric water vapour, calculated as the slope of the multi-model regression across CMIP6 and CCMI–2022 models between both quantities for each month (black) and from differencing the control and Lagrangian simulations of the targeted EMAC model experiment (red). Shown quantities are for (a) the NH and (b) the SH, and have been averaged over mid-latitudes in both hemispheres (50°–90°N/S) and over 150-200 hPa for water vapour. Solid symbols indicate months for which the correlations are statistically significant at the 95% level. Error bars show the min/max-range from inter-annual variability.

over the observation record could mask the long-term trend in the reanalysis while such variability could be underrepresented in the models. On the other hand, the climate models could overestimate the forced response of the extratropical tropopause.

Future tropopause pressure trends as simulated by CMIP6 and CCMI–2022 models strongly depend on the underlying greenhouse gas emission scenario. Figure 8c shows that these future trends are strongest at high latitudes, similar to simulated past trends. Averaged over mid-latitudes, the simulated future trends all show a tropopause rise (decreasing pressure), but with significant differences in magnitude ranging from around 0.5 %/dec for SSP2 and refD2, to around 1 %/dec for SSP2, and even around 1.5 %/dec for SSP5. There is also a significantly larger inter-model spread for the more extreme emission scenarios (cf. SSP5 to SSP2 in Figure 8d). At high latitudes, trends for individual models can reach extreme values of about 5 %/dec. The figure further shows that the model spread for a given emission scenario is of similar magnitude as the differences between different scenarios. Hence, model differences in the representation of atmospheric processes appear to substantially contribute to the uncertainty in future projections of the extratropical tropopause.

https://doi.org/10.5194/egusphere-2026-6385
Preprint. Discussion started: 30 October 2026
© Author(s) 2026. CC BY 4.0 License.

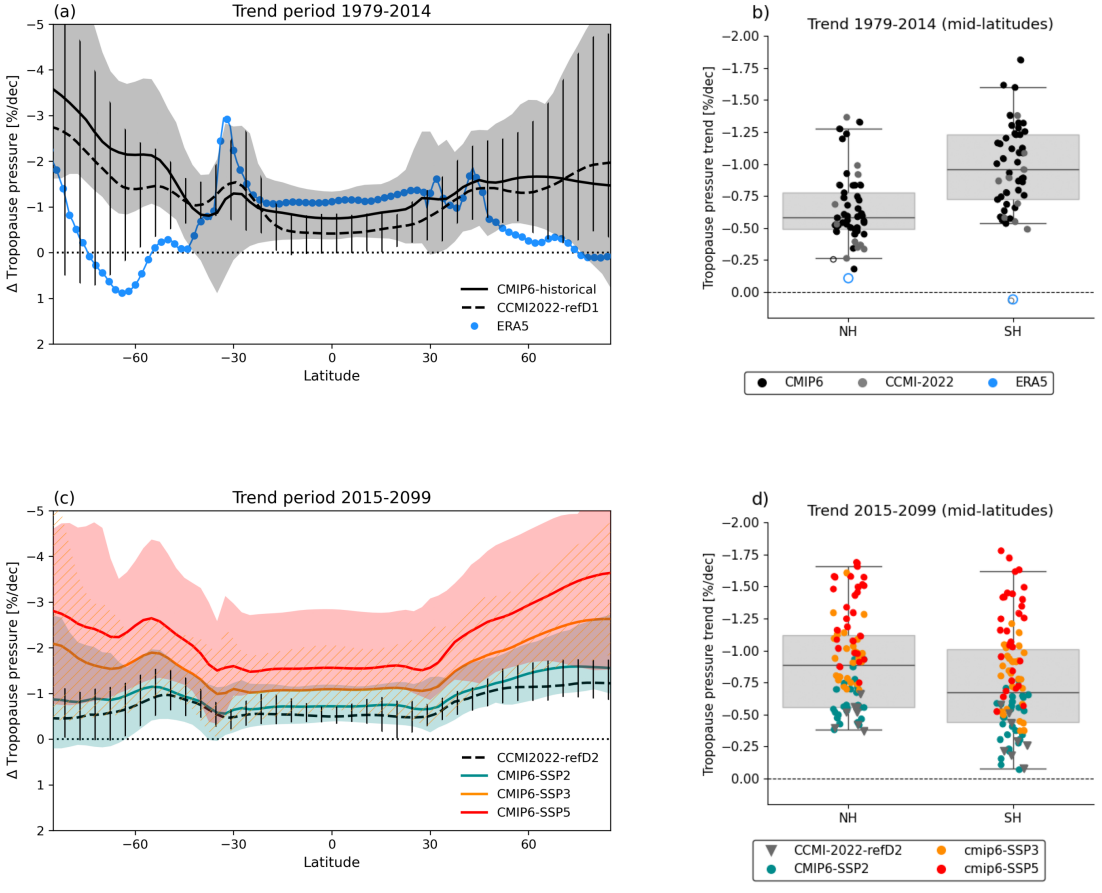

Figure 8. Trends of tropopause pressure over the past period 1979–2014 presented as (a) latitude profiles for CMIP6 (black solid the multi-model-mean, grey shading the min-max range) and CCMI–2022 black dashed the multi-model-mean, error bars the min-max range) as well as for ERA5 reanalysis. (b) Distribution of trend values for single models and ERA5 reanalysis averaged over mid-latitudes (50°-90°N/S). (c, d) Same, but for future trends over the period 2015–2099 and computed from CMIP6 SSP2 (green), SSP3 (orange), SSP5 (red) and CCMI–2022 refD2 (black) scenarios. Filled symbols in (b, d) indicate significance of the trend (p-value below 0.05). Grey shading shows the 25-75% percentile range, whiskers the approximate $\pm 2\sigma$-range of the CMIP6 and CCMI–2022 models.

6 Discussion and conclusions

We have shown that current climate models exhibit a significant low bias in the pressure of the climatological extratropical tropopause, corresponding to a high bias in tropopause height. The model simulations further show slightly reduced seasonal and inter-annual variability and stronger historical trends compared with ERA5 reanalysis. Multi-model statistics and a targeted

https://doi.org/10.5194/egusphere-2026-6385
Preprint. Discussion started: 30 October 2026
© Author(s) 2026. CC BY 4.0 License.

model experiment suggest that the substantial moist biases in the lowermost stratosphere in these models are the main factor for causing the tropopause height biases.

The documented biases in tropopause characteristics, potentially related to the moist bias in the lowermost stratosphere, may point to additional systematic biases in the models. For example, previous studies have shown evidence for changes in characteristics of the tropopause to be closely related to changes in the large-scale atmospheric circulation. Lorenz and DeWeaver (2007) analysed a suite of climate models in comparison with an idealized General Circulation Model (GCM) and showed that changes in mid-latitude circulation in a future climate with increased greenhouse warming are predominantly driven by a concomitant rise in the height of the extratropical tropopause. Their results suggest that a raised extratropical tropopause implies poleward shifts of the tropospheric eddy-driven jets. The mechanism involves strengthened eddy momentum and heat fluxes on the poleward side of the jet stream which, eventually, cause the poleward jet shift. While the rise in tropopause height, in turn, can be viewed as the response to some other forcing, the study by Lorenz and DeWeaver (2007) clearly demonstrates the strong connection between tropopause changes and variations in atmospheric circulation.

More recently, Boljka and Birner (2022) showed that current climate models generally simulate a slightly sharper tropopause than ERA5 reanalysis, although the comparison is complicated by differences in vertical resolution and the potential underestimation of tropopause sharpness in reanalyses. They argue that an increased tropopause sharpness modifies the characteristics for propagation and breaking of Rossby waves, with consequences for large-scale circulations. In particular, the changes in wave-mean flow interaction result in an intensified general circulation and an equatorward shifted tropospheric jet. This connection between the structure of the tropopause layer and the general circulation becomes evident from both multi-model statistics and inter-annual variability in reanalysis data (cf. Boljka and Birner, 2022). It remains an open question to what extent biases in tropopause sharpness in climate models and their associated effects on large-scale circulation are linked to the models' moist bias in the lowermost stratosphere above the extratropical tropopause (cf. Fig. 3).

The difference in tropopause height between tropics and extratropics, the so-called "tropopause break", has been used as a metric to quantify the width of the tropics (Davis and Rosenlof, 2012; Martin et al., 2020). There is strong evidence that the width of the tropics changes in response to global warming such that the tropics widen over time (e.g. Seidel et al., 2008; Staten et al., 2018). The biases in extratropical tropopause height identified and analysed here may affect estimates of tropical width based on tropopause-break metrics in climate models.

In addition, biases in tropopause height in model simulations likely imply issues for stratospheric mass estimates and simulated composition. If the simulated tropopause is too high, the stratosphere contains less mass relative to the troposphere in the simulation. Consequently, model estimates of dry air or tracer mass of the lowermost stratosphere, which are an important diagnostic for stratospheric composition (e.g. Weyland et al., 2025), are expected to be biased low. If less mass is contained in the stratosphere due to tropopause height biases, less mass of chemical species is recirculated through the stratosphere by the stratospheric circulation. A possible implication of such reduced recirculation could be reduced photochemical loss of certain chemical species (e.g. CFCs) at higher altitudes and related biases in simulated stratospheric composition.

As the height of the tropopause is affected by a variety of different factors it is a challenging question to what degree variations in tropopause height are caused by variations in the water vapour content of the lowermost stratosphere. It was

https://doi.org/10.5194/egusphere-2026-6385
Preprint. Discussion started: 30 October 2026
© Author(s) 2026. CC BY 4.0 License.

argued already by Held (1982) that the tropopause forms as the transition level between a dynamically active troposphere and a stratosphere in radiative balance. In addition, following studies emphasized the important role of the stratospheric circulation for determining a high tropopause in the tropics and a relatively low tropopause in the extratropics (e.g. Birner, 2010). Idealized models have been developed and shown to reliably simulate the height of the tropopause based on these processes (e.g. Thuburn and Craig, 2000; Hu and Vallis, 2019).

The radiative effects of water vapour in the lowermost stratosphere are only one factor influencing the stratospheric radiative balance, which in turn is only one of several factors affecting tropopause height. Hence, at first glance it might appear debatable that it is this factor which is most relevant for the substantial biases in the height of the extratropical tropopause as simulated by current climate models. However, the targeted EMAC model experiment allows an unambiguous attribution of the climatological tropopause high bias to the lowermost stratospheric water vapour moist bias. As the only difference between the EMAC control and the EMAC–CLaMS Lagrangian sensitivity simulations is the representation of stratospheric water vapour, all the differences between these simulations can clearly be attributed to the respective differences in stratospheric water vapour. In particular, lowermost stratospheric water vapour and the extratropical tropopause in the EMAC control simulation are representative for the moist-biased CMIP6 and CCMI–2022 climate model simulations, whereas the Lagrangian sensitivity simulation exhibits substantially reduced biases in both stratospheric water vapour and tropopause characteristics. The differences between the two simulations in the EMAC model experiment show a clear dependency of tropopause pressure on lowermost stratospheric water vapour, with the related difference in tropopause pressure of similar magnitude as the tropopause pressure biases in the other models (cf. Fig. 2). Also, the sensitivity of tropopause pressure to changes in lowermost stratospheric water vapour in the EMAC experiment is very similar to the multi-model analysis. Overall, the water vapour biases in the lowermost stratosphere in current climate model simulations are extreme (about 300% and more) and are indeed one of the most substantial biases in the UTLS region in the models. Given the close agreement of tropopause sensitivity with lowermost stratospheric water vapour between the EMAC experiment and the other models, we consider it very likely that also in the CMIP6 and CCMI–2022 simulations it is the moist bias in water vapour in the lowermost stratosphere which strongly contributes to the high bias in the extratropical tropopause.

It is another interesting question, to what degree the trends in tropopause height are related to trends in lowermost stratospheric water vapour. While it is well established that the tropopause rises in a future climate in response to CO_2-induced tropospheric warming and stratospheric cooling (e.g. Hu and Vallis, 2019), its relationship with changes in stratospheric water vapour has received comparatively little attention. Here, we can draw no conclusions if the simulated water vapour increase with global warming in a future climate (e.g. Banerjee et al., 2019) causes the rise of the tropopause, or if the rising tropopause (e.g. due to warming and changing dynamics in the troposphere) implies increasing water vapour mixing ratios at a given pressure level in the lowermost stratosphere. Targeted model experiments for a future climate scenario with locked and unlocked stratospheric water vapour would be needed to gain further insights into this question. Similarly, simplified mechanistic models (cf. Thuburn and Craig, 2000; Hu and Vallis, 2019) could be an efficient opportunity to investigate links between stratospheric water vapour (and also other trace constituents) and tropopause structure.

https://doi.org/10.5194/egusphere-2026-6385
Preprint. Discussion started: 30 October 2026
© Author(s) 2026. CC BY 4.0 License.

Overall, given the known links between tropopause structure and large-scale atmospheric circulation, as discussed above, we consider an accurate representation of the extratropical tropopause in climate models essential for reliable simulation of atmospheric circulation. Climate models robustly simulate a rising tropopause in a future warming climate, particularly under high-emission scenarios, alongside projected changes in atmospheric circulation, such as shifts in the jet streams. The fact that these models simulate large tropopause biases for the present climate, as shown here, raises questions about the reliability of their future projections of tropopause changes and related implications. In particular the significant inter-model spread in projected tropopause rise (cf. Fig. 8) could be related to substantial uncertainty in model projections of atmospheric circulation and transport. Our results suggest that improving the representation of stratospheric water vapour in climate models is a promising pathway toward a more realistic simulation of tropopause structure and atmospheric circulation in both present-day and future climates.

Code availability. The EMAC and EMAC–CLaMS models are available in the Modular Earth Submodel System (MESSy) git database. Detailed information is available at https://messy-interface.org/licence/application. Additional CLaMS software is available on a GitLab server at https://jugit.fz-juelich.de/clams/CLaMS (last access: 18 May 2026).

Data availability. ERA5 reanalysis data are available from the European Centre for Medium-range Weather Forecasts (https://apps.ecmwf.int/data-catalogues/era5/?class=ea, last access: 14 October 2026). The EMAC and EMAC–CLaMS model data used for this paper may be requested from the corresponding author (f.ploeger@fz-juelich.de). CMIP6 model data is publically available at https://esgf-node.llnl.gov/search/cmip6 (last access: 14 October 2026) and CCMI–2022 data at https://data.ceda.ac.uk/badc/ccmi/data/post-cmip6/ccmi-2022 (last access: 18 April 2026). SWOOSH data is publicly available at https://csl.noaa.gov/swoosh/ (last access: 14 October 2026).

Appendix A: Tropopause calculation

As climate model data are often available only as monthly mean fields, multi-model analyses, such as the one presented here, can only be performed using monthly mean data. We estimated the potential bias in thermal tropopause pressure arising from the use of monthly mean versus instantaneous data by calculating the tropopause fields for both cases for ERA5 reanalysis and the EMAC simulations, for which 6-hourly data was available. Figure A1 shows the climatological tropopause pressure for ERA5, EMAC and EMAC–CLaMS calculated from monthly mean and 6-hourly data and for DJF and JJA. In most cases, the tropopause is located a little higher if calculated from monthly mean fields, but these differences are much smaller than the differences between the different models. Hence, we conclude that the usage of either monthly mean or 6-hourly fields for tropopause calculation has a negligible effect on the results and conclusions presented in this paper.

https://doi.org/10.5194/egusphere-2026-6385
Preprint. Discussion started: 30 October 2026
© Author(s) 2026. CC BY 4.0 License.

Appendix B: Tropopause temperature

Figure A2a, b compares tropopause temperatures between the models and the reanalysis and shows that the cold bias at the extratropical tropopause is about 5K for the multi-model-mean, although not as pronounced as the tropopause high-bias. In particular for CMIP6, ERA5 tropopause temperatures fall mostly within the minimum-maximum range of the models. The targeted EMAC model experiment shows that the LMS moist bias induces significant local cooling, reducing temperatures in the LMS by up to approximately 8K. Also in CMIP6 and CCMI–2022 models, the cold bias is likely related to the simulated moist bias in the LMS, as shown by Charlesworth et al. (2023) using statistical arguments. As a side note, at the tropical tropopause, the CMIP6 and CCMI–2022 multi-model means are in good agreement with ERA5. The tropical tropopause cold bias in EMAC is likely related to a simplified, climatological representation of ozone, which is an important factor for temperatures in the tropical tropopause layer (e.g. Gettelman et al., 2009; Charlesworth et al., 2019).

Figure A2c, d shows the potential temperature of the thermal tropopause for the different climate models compared to ERA5 reanalysis. Climate model differences relative to the reanalysis are smaller for the potential temperature of the extratropical tropopause than for tropopause pressure (compare Fig. 1). This better agreement between climate models and reanalysis in potential temperature compared to pressure is due to the tropopause cold bias in the models, which partly compensates for the tropopause pressure low bias.

Appendix C: Conceptual framework for tropopause sensitivity

The conceptual framework to explain the tropopause pressure sensitivity with respect to lowermost stratospheric temperature (c.f. Sect. 4) is based on Bland et al. (2024) and the differences in the targeted EMAC experiment. In this framework, we approximate the potential temperature profiles as

$$z_i(\theta) = a_i\,\theta + b_i\ , \tag{C1}$$

with piece-wise constant lapse rate in the troposphere and lower stratosphere (for $i \in \{t, s\}$), respectively (see Fig. A3). We further assume that the cooling perturbation only exists in the LMS such that the temperature remains unchanged in the troposphere and above an altitude of about $z_{\mathrm{st}} = 17.5\,\mathrm{km}$, and that the largest temperature perturbation occurs around $z_{\mathrm{LMS}} = 12.1\,\mathrm{km}$. These assumptions are motivated by the differences between the two simulations in the EMAC experiment, where the perturbation in lowermost stratospheric water vapour only changes the profile in the lowermost stratosphere. Figure A3 illustrates this situation and shows how the tropopause shifts upwards or downwards for a cooling (blue dashed) or warming (red) perturbation in the LMS.

Under these assumptions and with the tropopause approximated as the intersection of the tropospheric and stratospheric profiles, the relation between the tropopause pressure and temperature in the lowermost stratosphere $T_{\mathrm{LMS}} = T(z_{\mathrm{LMS}})$ can be estimated as

$$p_{\mathrm{trop}}(T_{\mathrm{LMS}}) = p_0 \cdot e^{-\frac{\alpha T_{\mathrm{LMS}} + \beta}{H\,(T_{\mathrm{LMS}} + \gamma)}}\ , \tag{C2}$$

https://doi.org/10.5194/egusphere-2026-6385
Preprint. Discussion started: 30 October 2026
© Author(s) 2026. CC BY 4.0 License.

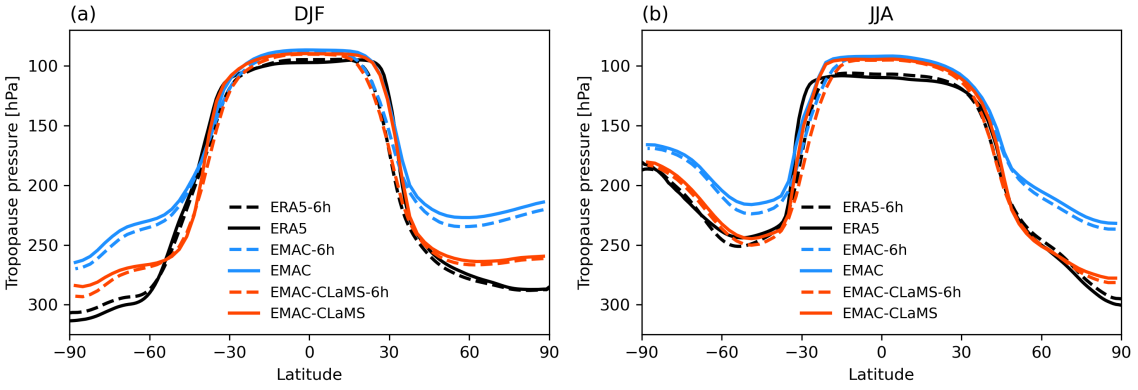

Figure A1. (Appendix figure) Sensitivity of thermal tropopause calculation with respect to temporal data resolution for (a) boreal winter (December–February) and (b) boreal summer (June–August). Shown is the climatological tropopause (2000–2014) calculated from monthly mean (solid) and from 6-hourly fields (dashed), for ERA5 reanalysis (black), EMAC control (blue) and Lagrangian EMAC–CLaMS climate model (red).

with $p_0 = 1000\,\text{hPa}$ the approximate surface pressure, $H = 7\,\text{km}$ a constant scale height and the coefficients α, β, γ defined by the constant parameters in the tropospheric reference temperature profile (Eq. C1) as

$$\alpha = z_{\text{st}}\,, \tag{C3}$$

$$\beta = \left[(z_{\text{st}} - z_{\text{LMS}})\left(\frac{b_t}{a_t}\right) - z_{\text{LMS}}\theta_{\text{st}}\right]\left(\frac{p_0}{p_{\text{LMS}}}\right)^{-\kappa}\,, \tag{C4}$$

$$\gamma = \left[\frac{z_{\text{st}} - z_{\text{LMS}}}{a_t} - \theta_{\text{st}}\right]\left(\frac{p_0}{p_{\text{LMS}}}\right)^{-\kappa}\,. \tag{C5}$$

Here, $\kappa = 0.286$ and the coefficients α, β, γ are defined by the constant parameters in the tropospheric reference temperature profile (Eq. C1). Also, p_{LMS} is the pressure in the LMS corresponding to z_{LMS} (assuming an exponential relationship with constant scale height $H = 7\,\text{km}$), and the choices of $z_{\text{st}} = 17.5\,\text{km}$, $z_{\text{LMS}} = 12.1\,\text{km}$ (and corresponding potential temperatures θ_{st} of 446 K and 442 K in the NH and SH, respectively), $a_t = 0.218\,\text{km/K}$ (in the NH), $a_t = 0.231\,\text{km/K}$ (in the SH), $b_t = -59.6\,\text{km}$ (in the NH) and $b_t = -62.78\,\text{km}$ (in the SH) are consistent with the difference between the two simulations in the EMAC experiment. The idealized relation of tropopause pressure as a function of lowermost stratospheric temperature, as given by Eq. C2, is shown as a red line in Fig. 6, in comparison to the multi-model statistics.

Author contributions. FP initiated the study, carried out parts of the analysis and wrote the manuscript. AM worked out the conceptual model and carried out further sensitivity experiments. HE and HW carried out parts of the analysis. SD and TB helped with preparing data and interpretation of the results. All authors contributed to the interpretation through many discussions and to writing the manuscript.

https://doi.org/10.5194/egusphere-2026-6385
Preprint. Discussion started: 30 October 2026
© Author(s) 2026. CC BY 4.0 License.

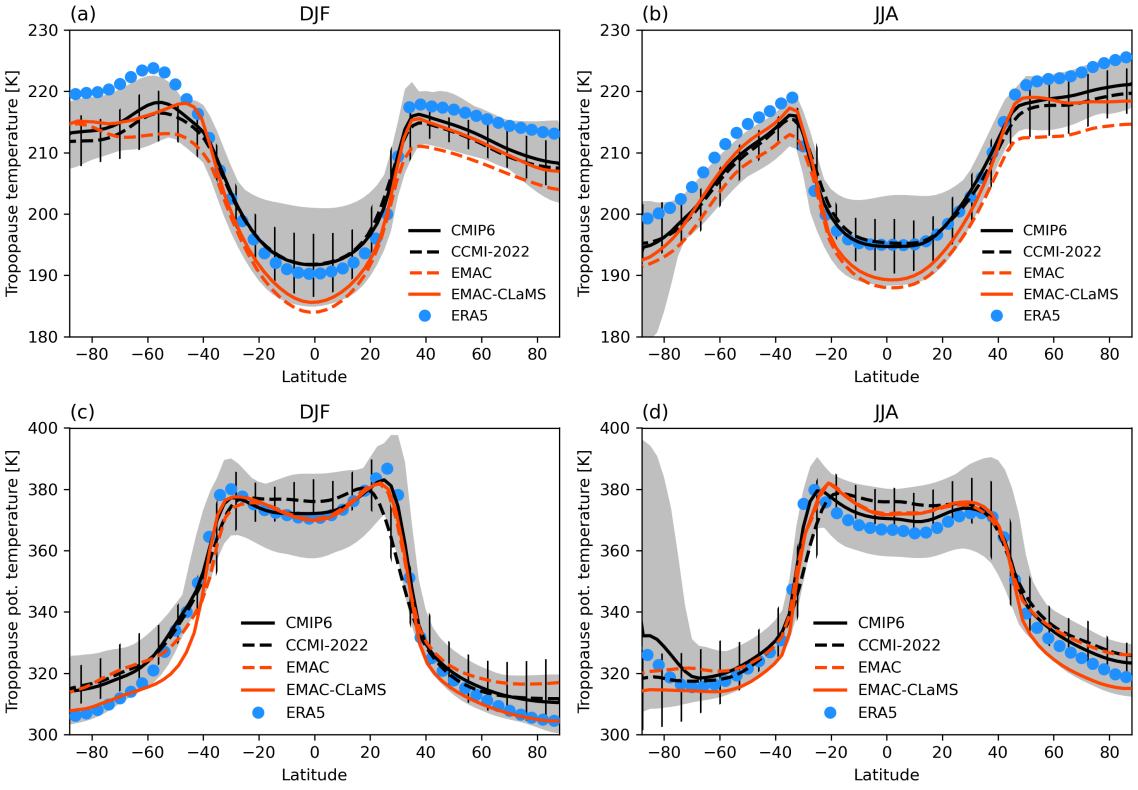

Figure A2. Climatological thermal tropopause temperature during (a) boreal winter (December–February, DJF) and (b) boreal summer (June–August). Data is shown from ERA5 reanalysis (blue), CMIP6 climate models (black solid line the multi-model-mean, grey shading the min-max range), CCMI–2022 models (black dashed, error bars the min-max range), targeted EMAC (red dashed) and EMAC–CLaMS (red solid) simulations. (c, d) Same, but for tropopause potential temperature.

Competing interests. There are no competing interests to declare.

Acknowledgements. This study was funded by the Deutsche Forschungsgemeinschaft (DFG, German Research Foundation) – TRR 301 – project-ID 428312742 and by the International Space Science Institute (ISSI) team "Climate effects of lowermost stratospheric water vapour" (project-ID 24-620). We acknowledge the modeling groups for making their simulations available for this analysis, the joint WCRP SPARC/IGAC Chemistry-Climate Model Initiative (CCMI) for organizing and coordinating the model data analysis activity, and the Centre for Environmental Data Analysis (CEDA) for collecting and archiving the CCMI model output. We further gratefully acknowledge the computing time for the CLaMS simulations which was granted on the supercomputer JURECA at the Jülich Supercomputing Centre (JSC) under the VSR project ID CLAMS–ESM.

https://doi.org/10.5194/egusphere-2026-6385
Preprint. Discussion started: 30 October 2026
© Author(s) 2026. CC BY 4.0 License.

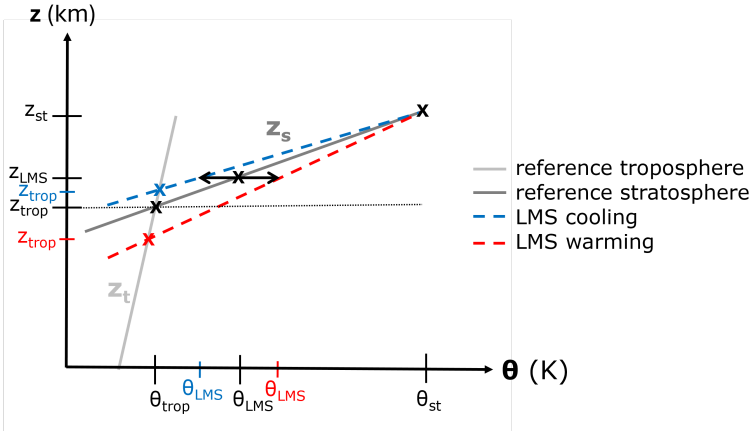

Figure A3. Schematic of the conceptual framework for the relation between tropopause pressure and lowermost stratospheric (LMS) temperature, in response to lowermost stratospheric cooling (see text). Reference potential temperature profile in grey, with tropospheric and stratospheric parts of the profile with constant lapse rates, respectively. Perturbed profiles due to cooling/warming in the LMS are shown as dashed blue/red lines. The tropospheric and stratospheric overworld profiles (above an altitude z_{st}) are assumed to remain unchanged under the perturbation, such that only the LMS part of the profile changes. The respective tropopause altitude and potential temperature is indicated by a cross.

References

Abalos, M., Birner, T., Chrysanthou, A., Davis, S., de la Cámara, A., Dhomse, S., Garny, H., Hegglin, M. I., Hubert, D., Ivaniha, O., Keeble, J., Linz, M., Minganti, D., Neu, J., Plummer, D., Saunders, L., Shah, K., Stiller, G., Tourpali, K., Waugh, D., Abraham, N. L., Akiyoshi, H., Chipperfield, M. P., Jöckel, P., Josse, B., Marchand, M., Martineau, P., Morgenstern, O., Sukhodolov, T., Watanabe, S. and Yamashita, Y.: Evaluation of stratospheric transport in three generations of Chemistry-Climate Models, Atmos. Chem. Phys., 26, 5249–5291, https://doi.org/10.5194/acp-26-5249-2026, 2026.

Banerjee, A., Chiodo, G., Previdi, M., Ponater, M., Conley, A. J., and Polvani, L. M.: Stratospheric water vapor: an important climate feedback, Climate Dynamics, 53, 1697–1710, https://doi.org/10.1007/s00382-019-04721-4, 2019.

Bauchinger, S., Engel, A., Jesswein, M., Keber, T., Bönisch, H., Obersteiner, F., Zahn, A., Emig, N., Hoor, P., Lachnitt, H.-C., Weyland, F., Ort, L., and Schuck, T. J.: The extratropical tropopause – trace gas perspective on tropopause definition choice, acp, 25, 14 167–14 186, https://doi.org/10.5194/acp-25-14167-2025, 2025.

Bethan, S., Vaughan, G., and Reid, S. J.: A comparison of ozone and thermal tropopause heights and the impact of tropopause definition on quantifying the ozone content of the troposphere, Q. J. R. Meteorol. Soc., 122, 929–944, https://doi.org/10.1002/qj.49712253207, 1996.

Birner, T.: Residual Circulation and Tropopause Structure, J. Atmos. Sci., 67, 2582–2600, https://doi.org/10.1175/2010JAS3287.1, 2010.

Birner, T., Dörnbrack, A., and Schumann, U.: How sharp is the tropopause at midlatitudes?, Geophys. Res. Lett., 29, https://doi.org/10.1029/2002GL015142, 2002.

Bland, J., Forbes, R., Gray, S. L., and Methven, J.: Processes controlling extratropical near-tropopause humidity and temperature in the ECMWF global weather forecast model, Q. J. R. Meteorol. Soc., 150, 5356–5372, https://doi.org/10.1002/qj.4873, 2024.

https://doi.org/10.5194/egusphere-2026-6385
Preprint. Discussion started: 30 October 2026
© Author(s) 2026. CC BY 4.0 License.

Boljka, L. and Birner, T.: Potential impact of tropopause sharpness on the structure and strength of the general circulation, npj Climate and Atmospheric Science, 5, 98, https://doi.org/10.1038/s41612-022-00319-6, 2022.

Brewer, A. W.: Evidence for a world circulation provided by the measurements of helium and water vapour distribution in the stratosphere, Q. J. R. Meteorol. Soc., 75, 351–363, https://doi.org/10.1002/qj.49707532603, 1949.

Charlesworth, E. J., Birner, T., and Albers, J. R.: Ozone transport-radiation feedbacks in the tropical tropopause layer, Geophys. Res. Lett., 46, 14195–14202, https://doi.org/10.1029/2019GL084679, 2019.

Charlesworth, E., Ploeger, F., Birner, T., Baikhadzhaev, R., Abalos, M., Abraham, L., Akiyoshi, H., Bekki, S., Dennison, F., Jöckel, P., Keeble, J., Kinnison, D., Morgenstern, O., Plummer, D., Rozanov, E., Strode, S., Zeng, G., and Riese, M.: Stratospheric water vapor affecting atmospheric circulation, Nat. Commun., 14, 3925, https://doi.org/10.1038/s41467-023-39559-2, 2023.

Davis, S. M. and Rosenlof, K. H.: A Multidiagnostic Intercomparison of Tropical-Width Time Series Using Reanalyses and Satellite Observations, Journal of Climate, 25, 1061–1078, https://doi.org/10.1175/JCLI-D-11-00127.1, 2012.

Davis, S. M., Rosenlof, K. H., Hassler, B., Hurst, D. F., Read, W. G., Vömel, H., Selkirk, H., Fujiwara, M., and Damadeo, R.: The Stratospheric Water and Ozone Satellite Homogenized (SWOOSH) database: a long-term database for climate studies, Earth System Science Data, 8, 461–490, https://doi.org/10.5194/essd-8-461-2016, 2016.

Eyring, V., Bony, S., Meehl, G. A., Senior, C. A., Stevens, B., Stouffer, R. J., and Taylor, K. E.: Overview of the Coupled Model Intercomparison Project Phase 6 (CMIP6) experimental design and organization, Geoscientific Model Development, 9, 1937–1958, https://doi.org/10.5194/gmd-9-1937-2016, 2016.

Fueglistaler, S., Bonazzola, M., Haynes, P. H., and Peter, T.: Stratospheric water vapor predicted from the Lagrangian temperature history of air entering the stratosphere in the tropics, J. Geophys. Res., 110, D08107, https://doi.org/10.1029/2004JD005516, 2005.

Gettelman, A., Birner, T., Eyring, V., Akiyoshi, H., Bekki, S., Brühl, C., Dameris, M., Kinnison, D. E., Lefevre, F., Lott, F., Mancini, E., Pitari, G., Plummer, D. A., Rozanov, E., Shibata, K., Stenke, A., Struthers, H., and Tian, W.: The tropical tropopause layer 1960–2100, Atmos. Chem. Phys., 9, 1621–1637, https://doi.org/10.5194/acp-9-1621-2009, 2009.

Gettelman, A., Hegglin, M. I., Son, S.-W., Kim, J., Fujiwara, M., Birner, T., Kremser, S., Rex, M., Añel, J. A., Akiyoshi, H., Austin, J., Bekki, S., Braesicke, P., Brühl, C., Butchart, N., Chipperfield, M., Dameris, M., Dhomse, S., Garny, H., Hardiman, S. C., Jöckel, P., Kinnison, D. E., Lamarque, J. F., Mancini, E., Marchand, M., Michou, M., Morgenstern, O., Pawson, S., Pitari, G., Plummer, D., Pyle, J. A., Rozanov, E., Scinocca, J., Shepherd, T. G., Shibata, K., Smale, D., Teyssèdre, H., and Tian, W.: Multimodel assessment of the upper troposphere and lower stratosphere: Tropics and global trends, J. Geophys. Res., 115, D00M08, https://doi.org/10.1029/2009JD013638, 2010.

Gettelman, A., Hoor, P., Pan, L. L., Randel, W. J., Hegglin, M. I., and Birner, T.: The extratropical upper troposphere and lower stratosphere, Rev. Geophys., 49, RG3003, https://doi.org/10.1029/2011RG000355, 2011.

Haqq-Misra, J., Lee, S., and Frierson, D. M. W.: Tropopause structure and the role of eddies, J. Atmos. Sci., 68, 2930–2944, https://doi.org/10.1175/JAS-D-11-087.1, 2011.

Haynes, P., Scinocca, J., and Greenslade, M.: Formation and maintenance of the extratropical tropopause by baroclinic eddies, Geophys. Res. Lett., 28, 4179–4182, https://doi.org/10.1029/2001GL013485, 2001.

Held, I. M.: On the Height of the Tropopause and the Static Stability of the Troposphere, J. Atmos. Sci., 39, 412–417, https://doi.org/10.1175/1520-0469(1982)039<0412:OTHOTT>2.0.CO;2, 1982.

Hegglin, M. I., Gettelman, A., Hoor, P., Krichevsky, R., Manney, G. L., Pan, L. L., Son, S.-W., Stiller, G., Tilmes, S., Walker, K. A., Eyring, V., Shepherd, T. G., Waugh, D., Akiyoshi, H., Añel, J. A., Austin, J., Baumgaertner, A., Bekki, S., Braesicke, P., Brühl, C., Butchart, N.,

https://doi.org/10.5194/egusphere-2026-6385
Preprint. Discussion started: 30 October 2026
© Author(s) 2026. CC BY 4.0 License.

Chipperfield, M., Dameris, M., Dhomse, S., Frith, S., Garny, H., Hardiman, S. C., Jöckel, P., Kinnison, D. E., Lamarque, J. F., Mancini, E., Michou, M., Morgenstern, O., Nakamura, T., Olivié, D., Pawson, S., Pitari, G., Plummer, D. A., Pyle, J. A., Rozanov, E., Scinocca, J. F., Shibata, K., Smale, D., Teyssèdre, H., Tian, W., and Yamashita, Y.: Multimodel assessment of the upper troposphere and lower stratosphere: Extratropics, J. Geophys. Res., 115, D00M09, https://doi.org/10.1029/2010JD013884, 2010.

Hersbach, H., Bell, B., Berrisford, P., Hirahara, S., Horànyi, A., Muñoz Sabater, J., Nicolas, J., Peubey, C., Radu, R., Schepers, D., Simmons, A., Soci, C., Abdalla, S., Abellan, X., Balsamo, G., Bechtold, P., Biavati, G., Bidlot, J., Bonavita, M., De Chiara, G., Dahlgren, P., Dee, D., Diamantakis, M., Dragani, R., Flemming, J., Forbes, R., Fuentes, M., Geer, A., Haimberger, L., Healy, S., Hogan, R. J., Hólm, E., Janisková, M., Keeley, S., Laloyaux, P., Lopez, P., Lupu, C., Radnoti, G., de Rosnay, P., Rozum, I., Vamborg, F., Villaume, S., and Thépaut, J.-N.: The ERA5 global reanalysis, Q. J. R. Meteorol. Soc., 146, 1999–2049, https://doi.org/10.1002/qj.3803, 2020.

Holton, J. R., Haynes, P., McIntyre, M. E., Douglass, A. R., Rood, R. B., and Pfister, L.: Stratosphere-troposphere exchange, Rev. Geophys., 33, 403–439, https://doi.org/10.1029/95RG02097, 1995.

Homeyer, C. R., Smith, J. B., Bedka, K. M., Bowman, K. P., Wilmouth, D. M., Ueyama, R., Dean-Day, J. M., St. Clair, J. M., Hannun, R., Hare, J., Pandey, A., Sayres, D. S., Hanisco, T. F., Gordon, A. E., and Tinney, E. N.: Extreme altitudes of stratospheric hydration by midlatitude convection observed during the DCOTSS field campaign, Geophys. Res. Lett., 50, e2023GL104 914, https://doi.org/10.1029/2023GL104914, 2023.

Homeyer, C. R. and Tinney, E. N.: Observed Long-Term Changes in Global Tropopause Characteristics, EGUsphere [preprint], https://doi.org/10.5194/egusphere-2026-3889, 2026.

Hu, S. and Vallis, G. K.: Meridional structure and future changes of tropopause height and temperature, Q. J. R. Meteorol. Soc., 145, 2698–2717, https://doi.org/10.1002/qj.3587, 2019.

Jöckel, P., Tost, H., Pozzer, A., Kunze, M., Kirner, O., Brenninkmeijer, C., Brinkop, S., Duy, S. C., Dyroff, C., Eckstein, J., Frank, F., Garny, H., Gottschaldt, K.-D., Graf, P., Grewe, V., Kerkweg, A., Kern, B., Matthes, S., Mertens, A., Meul, S., Neumaier, M., Nützel, M., Oberländer-Hayn, S., Ruhnke, R., Runde, T., Sander, R., Scharffe, D., and Zahn, A.: Earth System integrated Modelling (ESCiMo) with the Modular Earth Submodel System (MESSy) version 2.51, Geosci. Model Dev., 9, 1153–1200, https://doi.org/10.5194/gmd-9-1153-2016, 2016.

Keeble, J., Hassler, B., Banerjee, A., Checa-Garcia, R., Chiodo, G., Davis, S., Eyring, V., Griffiths, P. T., Morgenstern, O., Nowack, P., Zeng, G., Zhang, J., Bodeker, G., Burrows, S., Cameron-Smith, P., Cugnet, D., Danek, C., Deushi, M., Horowitz, L. W., Kubin, A., Li, L., Lohmann, G., Michou, M., Mills, M. J., Nabat, P., Olivie, D., Park, S., Seland, O., Stoll, J., Wieners, K.-H., and Wu, T.: Evaluating stratospheric ozone and water vapour changes in CMIP6 models from 1850 to 2100, acp, 21, 5015–5061, https://doi.org/10.5194/acp-21-5015-2021, 2021.

Kunz, A., Konopka, P., Müller, R., and Pan, L. L.: Dynamical tropopause based on isentropic potential vorticity gradients, J. Geophys. Res., 116, D01110, https://doi.org/10.1029/2010JD014343, 2011.

Lorenz, D. J. and DeWeaver, E. T.: Tropopause height and zonal wind response to global warming in the IPCC scenario integrations, J. Geophys. Res., 112, D10 119, https://doi.org/10.1029/2006JD008087, 2007.

Martin, E. R., Homeyer, C. R., McKinzie, R. A., McCarthy, K. M., and Xian, T.: Regionally Varying Assessments of Upper-Level Tropical Width in Reanalyses and CMIP5 Models Using a Tropopause Break Metric, Journal of Climate, 33, 5885–5903, https://doi.org/10.1175/JCLI-D-19-0629.1, 2020.

Nützel, M., Podglajen, A., Garny, H., and Ploeger, F.: Quantification of water vapour transport from the Asian monsoon to the stratosphere, Atmos. Chem. Phys., 19, 8947–8966, https://doi.org/10.5194/acp-19-8947-2019, 2019.

https://doi.org/10.5194/egusphere-2026-6385
Preprint. Discussion started: 30 October 2026
© Author(s) 2026. CC BY 4.0 License.

Park, M., Randel, W. J., Damadeo, R. P., Flittner, D. E., Davis, S. M., Rosenlof, K. H., et al.: Near-Global Variability of Stratospheric Water Vapor Observed by SAGE III/ISS, Journal of Geophysical Research: Atmospheres, 126, e2020JD034274, https://doi.org/10.1029/2020JD034274, 2021.

Ploeger, F., Günther, G., Konopka, P., Fueglistaler, S., Müller, R., Hoppe, C., Kunz, A., Spang, R., Grooß, J.-U., and Riese, M.: Horizontal water vapor transport in the lower stratosphere from subtropics to high latitudes during boreal summer, J. Geophys. Res., 118, 8111–8127, https://doi.org/10.1002/jgrd.50636, 2013.

Ploeger, F., Birner, T., Charlesworth, E., Konopka, P., and Müller, R.: Moist bias in the Pacific upper troposphere and lower stratosphere (UTLS) in climate models affects regional circulation patterns, Atmos. Chem. Phys., 24, 2033–2043, https://doi.org/10.5194/acp-24-2033-2024, 2024.

Plummer, D., Nagashima, T., Tilmes, S., Archibald, A. T., Chiodo, G., Fadnavis, S., Garny, H., Josse, B., Kim, J., Lamarque, J.-F., Morgenstern, O., Murray, L., Orbe, C., Tai, A. P. K., Chipperfield, M. P., Funke, B., Juckes, M., Kinnison, D., Kunze, M., Luo, B., Matthes, K., Newman, P. A., Pascoe, C., and Peter, T.: CCMI-2022: A new set of Chemistry–Climate Model Initiative (CCMI) community simulations to update the assessment of models and support upcoming Ozone Assessment activities, SPARC Newsletter, 57, 22–30, https://aparc-climate.org/newsletter/newsletter-archive/, 2021.

Pommrich, R., Müller, R., Grooß, J.-U., Konopka, P., Ploeger, F., Vogel, B., Tao, M., Hoppe, C. M., Günther, G., Spelten, N., Hoffmann, L., Pumphrey, H.-C., Viciani, S., D'Amato, F., Volk, C. M., Hoor, P., Schlager, H., and Riese, M.: Tropical troposphere to stratosphere transport of carbon monoxide and long-lived trace species in the Chemical Lagrangian Model of the Stratosphere (CLaMS), Geosci. Model Dev., 7, 2895–2916, https://doi.org/10.5194/gmd-7-2895-2014, 2014.

Randel, W. J., Wu, F., and Forster, P.: The Extratropical Tropopause Inversion Layer: Global Observations with GPS Data, and a Radiative Forcing Mechanism, Journal of the Atmospheric Sciences, 64, 4489–4496, https://doi.org/10.1175/2007JAS2412.1, 2007.

Randel, W. J. and Park, M.: Diagnosing Observed Stratospheric Water Vapor Relationships to the Cold Point Tropical Tropopause, Journal of Geophysical Research: Atmospheres, 124, 7018–7033, https://doi.org/10.1029/2019JD030648, 2019.

Reutter, P. and Spichtinger, P.: The frosty frontier: redefining the mid-latitude tropopause using the relative humidity over ice, acp, 25, 16 303–16 314, https://doi.org/10.5194/acp-25-16303-2025, 2025.

Rolf, C., Vogel, B., Hoor, P., Afchine, A., Günther, G., Krämer, M., Müller, R., Müller, S., Spelten, N., and Riese, M.: Water vapor increase in the lower stratosphere of the Northern Hemisphere due to the Asian monsoon anticyclone observed during the TACTS/ESMVal campaigns, Atmos. Chem. Phys., 18, 2973–2983, https://doi.org/10.5194/acp-18-2973-2018, 2018.

Schmidt, T., Cammas, J.-P., Smit, H. G. J., Heise, S., Wickert, J., and Haser, A.: Observational characteristics of the tropopause inversion layer derived from CHAMP/GRACE radio occultations and MOZAIC aircraft data, J. Geophys. Res., 115, D24304, https://doi.org/10.1029/2010JD014284, 2010.

Seidel, D. J. and Randel, W. J.: Variability and trends in the global tropopause estimated from radiosonde data, J. Geophys. Res., 111, D21 101, https://doi.org/10.1029/2006JD007363, 2006.

Seidel, D. J., Fu, Q., Randel, W. J., and Reichler, T. J.: Widening of the tropical belt in a changing climate, Nature, 1, 21–24, https://doi.org/10.1038/ngeo.2007.38, 2008.

Staten, P. W., Lu, J., Grise, K. M., Davis, S. M., and Birner, T.: Re-examining tropical expansion, Nature Climate Change, 8, 768–775, https://doi.org/10.1038/s41558-018-0246-2, 2018.

Thuburn, J. and Craig, G. C.: Stratospheric Influence on Tropopause Height: The Radiative Constraint, J. Atmos. Sci., 57, 17–28, https://doi.org/10.1175/1520-0469(2000)057<0017:SIOTHT>2.0.CO;2, 2000.

https://doi.org/10.5194/egusphere-2026-6385
Preprint. Discussion started: 30 October 2026
© Author(s) 2026. CC BY 4.0 License.

Tinney, E. N., Homeyer, C. R., Elizalde, L., Hurst, D. F., Thompson, A. M., Stauffer, R. M., Vömel, H., and Selkirk, H. B.: A Modern Approach to a Stability-Based Definition of the Tropopause, Monthly Weather Review, 150, 3151–3174, https://doi.org/10.1175/MWR-D-22-0174.1, 2022.

Turhal, K., Plöger, F., Clemens, J., Birner, T., Weyland, F., Konopka, P., and Hoor, P.: Variability and trends in the potential vorticity (PV)-gradient dynamical tropopause, acp, 24, 13 653–13 679, https://doi.org/10.5194/acp-24-13653-2024, 2024.

Ueyama, R., Schoeberl, M., Jensen, E., Pfister, L., Park, M., and Ryoo, J.-M.: Convective Impact on the Global Lower Stratospheric Water Vapor Budget, Journal of Geophysical Research: Atmospheres, 128, e2022JD037135, https://doi.org/10.1029/2022JD037135, 2023.

Weyland, F., Hoor, P., Kunkel, D., Birner, T., Plöger, F., and Turhal, K.: Long-term changes in the thermodynamic structure of the lowermost stratosphere inferred from reanalysis data, Atmos. Chem. Phys., 25, 1227–1252, https://doi.org/10.5194/acp-25-1227-2025, 2025.

WMO: Meteorology–A three-dimensional science, WMO Bull, pp. 134–138, https://library.wmo.int/idurl/4/42003, 1957.

World Meteorological Organization (WMO): Scientific Assessment of Ozone Depletion: 2022, GAW Report No. 278, 509 pp., WMO, Geneva, https://ozone.unep.org/sites/default/files/2023-02/Scientific-Assessment-of-Ozone-Depletion-2022.pdf, 2022.